Rotational Spectroscopic and ab Initio Studies of the Xe−H_2O van der Waals Dimer

Qing Wen and Wolfgang Jäger*

Department of Chemistry, University of Alberta, Edmonton AB T6G 2G2, Canada

Received: March 30, 2006; In Final Form: April 24, 2006

An ab initio potential energy surface of the Xe−H_2O van der Waals dimer was constructed at the coupled cluster level of theory with single, double, and pertubatively included triple excitations. For the Xe atom, the small-core pseudopotential and augmented correlation-consistent polarized valence quadruple-ζ (aug-cc-pVQZ-PP) basis set was used. Dunning's augmented correlation-consistent polarized valence triple-ζ (aug-cc-pVTZ) basis set was chosen for O and H atoms. Midbond functions were used to supplement the atom-centered basis sets. Rotational spectra of the Xe−H_2O van der Waals dimer were recorded with a pulsed-nozzle Fourier transform microwave spectrometer. Rotational transitions within two internal rotor states, namely, the $\sum 0_{00}$ and $\sum 1_{01}$ states, were measured and assigned. Nuclear quadrupole hyperfine structures due to the ^{131}Xe ($I = {}^3/_2$), D ($I = 1$) and ^{17}O ($I = {}^5/_2$) nuclei were also observed and analyzed. Information about the molecular structure and the H_2O angular motions was extracted from the spectroscopic results with the assistance of the ab initio potential.

I. Introduction

Xenon has become an important probe in nuclear magnetic resonance (NMR) spectroscopy, where it is used in high-resolution imaging applications of, for example, materials and biological tissues.[1,2] For ^{129}Xe and ^{131}Xe, which have nonzero nuclear spins, high spin polarizations can be achieved using an optical pumping scheme to significantly increase the NMR signals.[1,3] The in vivo applications, to obtain, for example, images of the brain, blood, and lung space are of particular interest because of their potential in clinical use to aid in the diagnosis and treatment of a number of pathological conditions. Also, the large and sensitive chemical shifts of ^{129}Xe and ^{131}Xe make these nuclei an ideal atomic probe for the characterization of microporous materials, such as zeolites, to obtain the information about the dimension and the adsorption ability of the pores.[4]

Detailed information about Xe−molecule interactions is essential for the interpretation of Xe NMR data.[5] For example, accurate interaction potentials are an important ingredient for the construction of magnetic shielding surfaces. We have recently studied the Xe−N_2 (ref 6) and Xe−CH_4 (ref 7) van der Waals complexes using experimental spectroscopic and ab initio computational methods, to contribute to the understanding of xenon−molecule interactions. Ab initio interaction potentials were constructed and used to complement the rotational spectroscopic results to obtain the information about molecular structure and dynamics, for example, the intermolecular stretching and bending motions. Good consistency was found between the spectroscopic and ab initio results. For Xe−N_2 (ref 6), the resulting scaled ab initio potential can reproduce the microwave rotational spectra to within 0.01%. These studies, together with previously reported microwave investigations of Xe atom/molecule dimers, including Rg−Xe (Rg = Ne, Ar, and Kr),[8] Xe−HCl,[9,10] Xe−HF,[11] Xe−CO_2,[12] Xe−CO,[13] and Xe−C_6H_6,[14] provided detailed probes into the nature of Xe−molecule intermolecular forces and might help to understand more complex Xe−host site interactions.

The present study of the Xe−H_2O complex is part of our continuing research of the Xe−molecule interaction and is based on two motivations: (1) Water exists in great quantities in the human body. Detailed insight into the Xe−H_2O interaction will provide a basis for an interpretation of the background signal in in vivo NMR images contributed by the water. (2) Xe−H_2O can be regarded as a prototypical model for hydrophobic interactions, an important intermolecular interaction in many biological systems. An accurate potential for Xe−H_2O will be a starting point for a better understanding of the interactions of xenon atoms in biological systems.

A number of interaction potentials for Ar−H_2O[15−20] and Kr−H_2O[21] complexes have been previously reported. These potentials all predict an equilibrium geometry in which all four atoms are coplanar. However, the angle θ between the intermolecular axis and the C_2 axis of the H_2O unit (see Figure 1) is not consistent among the different studies. For Ar−H_2O, an anti-hydrogen bonded orientation of the H_2O unit was found in a MP2 potential reported by Chalasinski et al.[18] and a semiempirical potential by Bulski et al.,[19] with $\theta = 100°$ and 129.5°, respectively. In contrast, Cohen et al.[17] determined an intermolecular potential using spectroscopic data, and a hydrogen bonded H_2O orientation ($\theta = 74.3°$) was found. This is in agreement with the MP4 potential energy surface ($\theta = 75°$) reported by Tao et al.[20] A similar equilibrium geometry was also found in the MP2 calculation of the Kr−H_2O ($\theta = 80°$) potential by Chalasinski et al.[21]

Extensive spectroscopic studies have been carried out on the Ar−H_2O[22−31] and Kr−H_2O[32] complexes, in both microwave and infrared regions. Two internal rotor states were observed in the microwave spectra,[22,23,32] in accord with computational studies.[17,20,21] For example, the Ar−H_2O potential by Cohen et al.[17] predicts that the H_2O in-plane rotation is hindered by barriers at $\theta = 0°$ (26.3 cm^{-1}) and $\theta = 180°$ (17.2 cm^{-1}), corresponding to the symmetric Ar−H_2O and Ar−OH_2 configurations, respectively. The out-of-plane rotation of H_2O is

* Corresponding author. Tel: 1-780-492-5020. Fax: 1-780-492-8231. E-mail: Wolfgang.Jaeger@ualberta.ca.

10.1021/jp0619890 CCC: $33.50 © 2006 American Chemical Society
Published on Web 06/01/2006

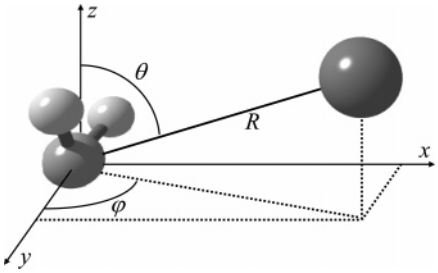

Figure 1. Molecule fixed axes frame for the Xe−H_2O complex. The origin of the coordinate system is at the center-of-mass of the H_2O unit, and the C_2 axis of H_2O is chosen as the *z*-axis. The H_2O unit lies in the *yz*-plane. The position of the Xe atom is described by spherical coordinates (R, θ, φ). R is the distance between Xe and the origin, θ is the angle between the R vector and the *z*-axis. $\theta = 0°$ corresponds to the C_{2v} geometry where the hydrogen atoms point to the xenon atom. φ is the angle for the H_2O out-of-plane rotation about its symmetry axis from a reference geometry ($\varphi = 0°$) in which all four atoms are coplanar. $\theta = 0°$, $\varphi = 0°$ corresponds to the symmetric Xe−H_2O geometry, and $\theta = 180°$, $\varphi = 0°$ corresponds to the symmetric Xe−OH_2 geometry. $\theta = 53°$, $\varphi = 0°$ corresponds to an L-shaped Xe−HOH structure with a linear Xe−HO arrangement.

hindered by a barrier of 54.2 cm^{-1} at $\theta = 90°$ and $\varphi = 90°$ (φ is the angle for H_2O out-of-plane rotation about its symmetry axis. $\varphi = 0°$ if all four atoms coplanar; see Figure 1). The microwave studies could determine effective structures and H_2O dynamics in these complexes. In both the Ar− and the Kr−H_2O case, the microwave data show that the hydrogen atoms point toward Ar or Kr in both observed states, and a large amplitude H_2O out-of-plane motion is present despite the high energy barrier.[22,23,32]

In this paper, we present both microwave and ab initio studies of the Xe−H_2O complex. A potential energy surface of Xe−H_2O was constructed at the comprehensive coupled cluster level of theory with single, double, and pertubatively included triple excitations [CCSD(T)]. Rotational transitions within two internal rotor states were measured using a Fourier transform microwave spectrometer. Nuclear quadruple hyperfine structures due to the ^{131}Xe, D and ^{17}O nuclei were also observed and analyzed. Information about the molecular structure and the H_2O angular motions was extracted from the spectroscopic results with the assistance of the ab initio potential.

II. Ab Initio Potential Energy Calculations

Potential energies were calculated using the MOLPRO 2002.6 package of ab initio programs[33] at the CCSD(T) level of theory.[34,35] For the Xe atom, the small-core pseudopotential and augmented correlation-consistent polarized valence quadruple-ζ (aug-cc-pVQZ-PP) basis set[36] was chosen. Dunning's augmented correlation-consistent polarized valence triple-ζ (aug-cc-pVTZ) basis set[37] was used for O and H atoms. Midbond functions (3s3p2d2f1g) were added at the midpoint of the van der Waals bond,[38,39] with the exponents α_s, $\alpha_p = 0.94, 0.34, 0.12$; α_d, $\alpha_f = 0.64, 0.23$; $\alpha_g = 0.35$. The potential energies were calculated using the supermolecule approach and the counterpoise correction[40] was applied to remove basis-set superposition error.[41]

The Xe−H_2O geometry is defined by a set of spherical polar coordinates (R, θ, φ), with the origin of the coordinate system at the center-of-mass of the H_2O monomer, as shown in Figure 1. The H_2O monomer was kept rigid at its equilibrium structure, with a O−H bond length of 0.9575 Å and a H−O−H angle of 104.51 degrees.[42] R is the distance between Xe and the center-of-mass of the H_2O unit and θ is the angle between the R vector and the symmetry axis of the H_2O monomer. $\theta = 0°$ corresponds to C_{2v} geometry where the hydrogen atoms point to the xenon atom. φ is the angle for the H_2O out-of-plane rotation about its symmetry axis from a reference geometry ($\varphi = 0°$) in which all four atoms are coplanar. The Xe−H_2O potential energy surface was constructed on a grid of 630 points. R was varied from 3.5 to 4.3 Å in steps of 0.1 Å, θ from 0° to 180° in steps of 10°, and φ from 0° to 90° in steps of 30°. The calculated interaction energies are given in Table S1 of the Supporting Information.

III. Experimental Details

The rotational spectra of the Xe−H_2O dimer were recorded with a Balle−Flygare type[43] Fourier transform microwave spectrometer described previously.[44] The molecular expansion travels parallel to the direction of the microwave propagation, and as a result, each transition appears as a Doppler doublet. The relatively small dipole moment of the Xe−H_2O dimer made it necessary to amplify the microwave excitation pulses with a 1 W solid-state amplifier. The observed spectral line widths are ~7 kHz (full width at half-maximum) and the estimated measurement uncertainty is ±1 kHz.

The Xe−H_2O complexes were generated and stabilized in a supersonic expansion of a gas mixture through a General Valve (Series 9) pulsed nozzle with circular orifice (diameter 0.8 mm). The rotational temperature of the molecular expansion was estimated to be lower than 1 K. The gas mixtures consisted of 0.1% H_2O vapor and 0.4% Xe in Ne at a total pressure of about 5 atm. Dimers containing five different isotopes of Xe were studied in their natural isotopic abundances (^{136}Xe: 8.87%, ^{134}Xe: 10.44%, ^{132}Xe: 26.89%, ^{131}Xe: 21.18%, ^{129}Xe: 26.44%). Isotopically enriched samples were used to investigate isotopomers containing D_2O (99.8%), $H_2{}^{17}O$ (35−40% ^{17}O, Cambridge Isotope Laboratories), and $H_2{}^{18}O$ (70% ^{18}O, Cambridge Isotope Laboratories). For Xe−HDO, the same sample mixtures as for Xe−D_2O were used because HDO can be generated through the fast exchange between D_2O and residual H_2O in the sample system. The intensities of Xe−HDO transitions were found to increase significantly after conditioning the sample system for 1−2 h.

IV. Spectroscopic Search, Assignments, and Analysis

The H_2O unit was anticipated to undergo large amplitude internal rotation motions within the Xe−H_2O dimer. As a consequence, transitions within different internal rotor states were expected to occur. Following the labeling scheme developed by Hutson[15] and Cohen et al.,[25] the two lowest energy tunneling states correlate with the $j_{kakc} = 0_{00}$ and 1_{01} states of free water, and are designated as $\Sigma 0_{00}$ and $\Sigma 1_{01}$ states, respectively. Σ represents $K = 0$ where K is the projection of the angular momentum of the H_2O monomer onto the intermolecular axis. Fermi−Dirac statistics applies for the isotopomers containing H_2O, requiring the total wavefuction to be antisymmetric with respect to the exchange of two hydrogen nuclei (angular momentum quantum number $I = {}^1/_2$). This results in the antisymmetric spin function ($I = 0$, para H_2O) to be associated with the symmetric $\Sigma 0_{00}$ tunneling state and symmetric spin function ($I = 1$, ortho H_2O) with the antisymmetric $\Sigma 1_{01}$ state. The isotopomers containing D_2O obey Boson−Einstein spin statistics and the total wave function must be symmetric with respect to the exchange of two deuterium nuclei ($I = 1$). Consequently, the $\Sigma 0_{00}$ state has total nuclear spins of 0 and 2, whereas the $\Sigma 1_{01}$ state has total spin of 1. The spin statistical weights for the $\Sigma 0_{00}$ and $\Sigma 1_{01}$ states are 1 and 3 for Xe−H_2O, and 6 and 3 for Xe−D_2O, respectively. For Xe−

H_2O and Xe−D_2O, the $\sum 1_{01}$ state is metastable because relaxation from the $\sum 1_{01}$ to $\sum 0_{00}$ state is a nuclear-spin-forbidden process. As a result, transitions within both these two internal rotor states were expected to be observed. For Xe−HDO, the $\sum 1_{01}$ state is no longer metastable because of the lower symmetry for the HDO unit, and only $\sum 0_{00}$ ground-state transitions were expected.

4.1. Xe−H_2O. We started the spectral search for Xe−H_2O with the $J = 2-1$ transitions around 8 GHz. Initial transition frequencies were predicted on the basis of a pseudodiatomic approximation. The separation between Xe and the center-of-mass of H_2O was estimated to be 3.97 Å by comparison of the corresponding distances in Kr−CO_2 and Xe−CO_2 (ref 12) with that in Kr−H_2O (ref 32) and extrapolation to Xe−H_2O. The $J = 2$-1 transition for the ^{132}Xe− H_2O isotopomer was predicted to be at 8104 MHz and two transitions were soon found at 8181 and 8022 MHz, with an intensity ratio of approximately 1:3. This intensity ratio is consistent with the spin statistical weights of 1 and 3 for the $\sum 0_{00}$ and $\sum 1_{01}$ states and transitions were assigned accordingly. The assignments were further supported by the observation of nuclear hyperfine splittings in the $J = 1$-0, $\sum 1_{01}$ transition, but not in the corresponding transition in the $\sum 0_{00}$ state. These hyperfine splittings could be due to the nuclear spin−spin, or spin−rotation interactions, which are expected only for $\sum 1_{01}$ state ($I = 1$). The hyperfine structure extends over about 50 kHz, the same order of magnitude as observed for Ar−H_2O.[23] We have tried hard to resolve the hyperfine structure for ^{132}Xe−H_2O, but without success. The rotational transition appears to be split into four to five possible hyperfine components (see Figure S1 of the Supporting Information) instead of three, given by a hyperfine prediction, which is similar to the observation in Ar−H_2S.[45] Other J transitions and transitions of complexes containing the five main Xe isotopes were located straightforwardly. Nuclear quadrupole hyperfine structure due to the presence of the ^{131}Xe ($I = {}^3/_2$) nucleus was also observed, which confirmed the assignment to the Xe-containing species. Example spectra of the ^{131}Xe nuclear quadrupole hyperfine structure are shown in Figure 2.

All measured transition frequencies are listed in Tables 1 and 2 together with the quantum number assignments. Pickett's SPFIT/SPCAT suite of programs[46] was used to determine the spectroscopic constants. For each internal rotor state, a pseudodiatomic approach was applied and values for the rotational constant B, centrifugal distortion constant D, and ^{131}Xe nuclear quadrupole coupling constants χ_{aa} were obtained (see Tables 1 and 2).

4.2. Xe−$H_2{}^{18}O$ and Xe−$H_2{}^{17}O$. The locations of Xe−$H_2{}^{18}O$ and Xe−$H_2{}^{17}O$ transitions were predicted using a pseudodiatomic approach with scaled reduced mass. The observed transition frequencies within two internal rotor states are listed in Tables S2 and S3 of the Supporting Information and in Table 3. The transition intensity ratio stays the same as for Xe−H_2O for these two states because their spin statistics are analogous. Because the $H_2{}^{18}O$ and $H_2{}^{17}O$ samples were only partially enriched, the observed transitions were less intense than those for isotopomers with normal H_2O. The transition intensities of Xe−$H_2{}^{17}O$ were further reduced by ^{17}O ($I = {}^5/_2$) nuclear hyperfine splittings, causing significant difficulties to measure and resolve the spectra. Due to these difficulties, only the $J = 2$-1 hyperfine transition frequencies within each internal rotor state for two main Xe isotopes (^{132}Xe and ^{129}Xe) were measured. The ^{17}O nuclear quadruple hyperfine structures were partially resolved and assigned. Figure 3 shows an example spectrum of the ^{132}Xe−$H_2{}^{17}O$ isotopomer in the $\sum 1_{01}$ state to demonstrate the signal-to-noise ratio achieved. The spectroscopic constants, including the ^{131}Xe nuclear quadrupole coupling constants, obtained for Xe−$H_2{}^{18}O$ are shown in Tables S2 and S3 of the Supporting Information. For Xe−$H_2{}^{17}O$, the rotational constant B and the ^{17}O nuclear quadrupole coupling constant χ_{aa} were determined (see Table 3). The centrifugal distortion constant D could not be obtained because only one transition was measured for each internal rotor state.

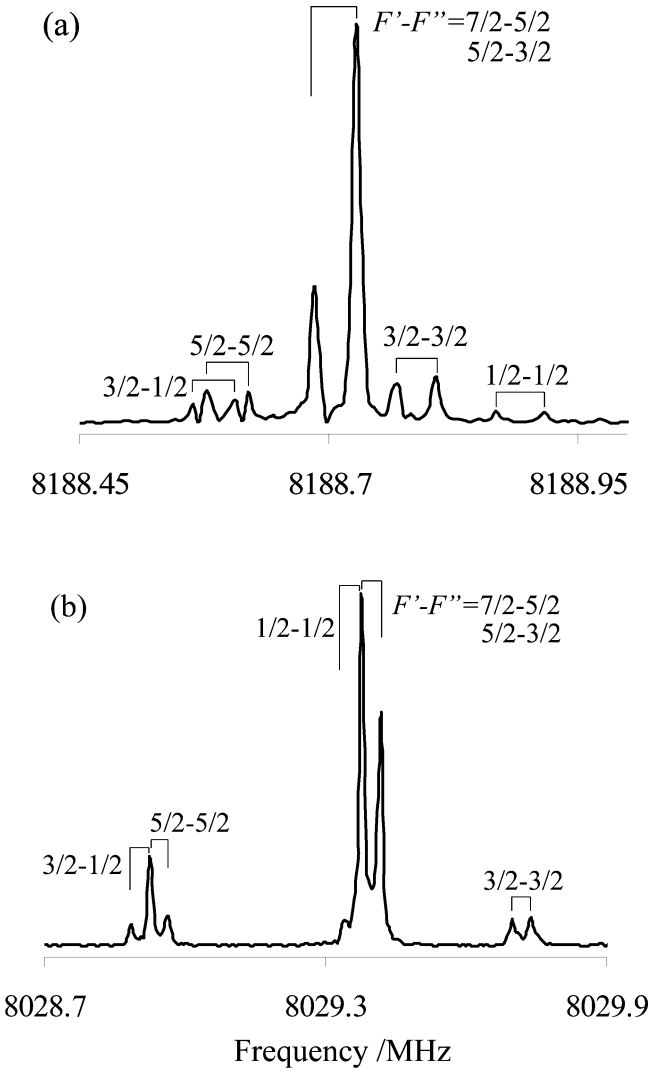

Figure 2. Composite spectra of the $J = 2$-1 transitions of the $\Sigma 0_{00}$ (a) and $\Sigma 1_{01}$ states (b) of ^{131}Xe−H_2O. (a) was recorded using 800 averaging cycles, and (b) using 100 averaging cycles.

4.3. Xe−D_2O. Two tunneling components for each J transition were also observed for the Xe−D_2O complexes because D_2O has the same symmetry as H_2O. We found that the higher frequency component is more intense than the lower frequency one. According to the spin statistical weights (6 and 3 for the $\sum 0_{00}$ and $\sum 1_{01}$ states, respectively), we assigned the higher frequency component to the $\sum 0_{00}$ state.

Both tunneling components show hyperfine structures due to D nuclear quadrupole interactions. The partially resolved hyperfine structures for the two tunneling states of the $J = 2$-1 transition are shown in Figure 4. Following the Boson−Einstein statistics, the $\sum 0_{00}$ state requires a total deuteron nuclear spin, I_D, of 0 and 2, whereas the $\sum 1_{01}$ state requires I_D to be 1. The hyperfine structure in the lower frequency component was found to match the $I_D = 1$ hyperfine pattern better, which further supported the assignment of the two internal rotor states.

TABLE 1: Measured Transition Frequencies and Spectroscopic Constants for Xe−H_2O Isotopomers

	^{136}Xe−H_2O		^{134}Xe−H_2O		^{132}Xe−H_2O		^{129}Xe−H_2O	
$J'-J''$	ν_{obs} (MHz)	$\Delta\nu^a$ (kHz)	ν_{obs} (MHz)	$\Delta\nu$ (kHz)	ν_{obs} (MHz)	$\Delta\nu$ (kHz)	ν_{obs} (MHz)	$\Delta\nu$ (kHz)
				$\Sigma 0_{00}$				
1-0	4076.7294	−0.06	4083.7680	−0.8	4091.0195	−1.0	4102.3064	−0.8
2-1	8152.7126	0.05	8166.7894	0.6	8181.2879	−0.5	8203.8596	0.7
3-2	12227.2029	−0.01	12248.3110	−0.2	12270.0524	1.3	12303.8994	−0.2
4-3					16356.5556	−0.5	16401.6739	0.02
B/MHz	2038.4269 (4)		2041.9468 (4)		2045.5730 (2)		2051.2166 (2)	
D/kHz	31.10(2)		31.20(2)		31.358(9)		31.479(9)	
δ/kHz[b]	0.04		0.6		0.9		0.5	
				$\Sigma 1_{01}$				
1-0	3997.6954	0.2	4004.4375	−2.2	4011.3860	−0.8	4022.2011	−0.3
2-1	7994.8759	−1.4	8008.3659	0.2	8022.2580	−0.7	8043.8850	−0.6
3-2	11991.0344	1.4	12011.2659	1.4	12032.1023	1.4	12064.5365	0.9
4-3	15985.6487	−0.4	16012.6218	−0.6	16040.3978	−0.5	16083.6340	−0.3
B/MHz	1998.8904 (2)		2002.2626 (2)		2005.7363 (2)		2011.1438 (2)	
D/kHz	21.382(9)		21.402(9)		21.454(9)		21.547(9)	
δ/kHz	1.0		1.3		0.9		0.6	

[a] $\Delta\nu = \nu_{obs} - \nu_{cal}$. [b] Standard deviation of the fit.

TABLE 2: Measured Transition Frequencies and Spectroscopic Constants, Including ^{131}Xe Nuclear Quadrupole Coupling Constants, of ^{131}Xe−H_2O

		$\Sigma 0_{00}$		$\Sigma 1_{01}$	
$J'-J''$	$F'-F''$	ν_{obs} (MHz)	$\Delta\nu$ (kHz)[a]	ν_{obs} (MHz)	$\Delta\nu$ (kHz)
1-0	1.5−1.5	4094.6347	0.9	4014.5704	−0.9
	2.5−1.5	4094.7445	−0.6	4015.0244	−0.3
	0.5−1.5	4094.8347	0.6	4015.3863	−1.2
2-1	1.5−0.5	8188.5777	−3.4	8028.8982	−0.8
	2.5−2.5	8188.5932	2.6	8028.9381	0.3
	0.5−0.5			8029.3512	−1.2
	2.5−1.5	8188.7023	0.5	8029.3924	1.1
	3.5−2.5	8188.7023	0.5	8029.3924	1.1
	1.5−1.5	8188.7810	−0.3	8029.7144	−0.8
	0.5−1.5	8188.8924	−0.2		
3-2	2.5−1.5	12281.1340	1.1	12042.6495	0.6
	1.5−0.5	12281.1340	1.1	12042.6495	0.6
	3.5−2.5	12281.1595	−0.9	12042.7626	1.5
	4.5−3.5	12281.1595	−0.9	12042.7626	1.5
	2.5−2.5			12042.9740	1.2
4-3	4.5−3.5			16054.5924	−1.2
	5.5−4.5			16054.5924	−1.2
B/MHz		2047.4242(2)		2007.5100(2)	
D/kHz		31.39(1)		21.484(7)	
$\chi_{aa}(^{131}Xe)$/MHz		−0.445(1)		−1.814(2)	
δ/kHz[b]		1.5		1.0	

[a] $\Delta\nu = \nu_{obs} - \nu_{cal}$. [b] Standard deviation of the fit.

All measured transition frequencies are listed in Table S4 and S5 of the Supporting Information, together with the spectroscopic constants, including the D nuclear quadrupole coupling constant. For ^{131}Xe−D_2O, several hyperfine components due to the ^{131}Xe nucleus were measured in the $\Sigma 0_{00}$ state. In the $\Sigma 1_{01}$ state, only the strongest component for each transition was observed due to the low signal-to-noise ratio achieved. However, the information was sufficient to determine the ^{131}Xe nuclear quadrupole coupling constants for both states (see Table S4 of the Supporting Information).

4.4. Xe−HDO. Only transitions within the $\Sigma 0_{00}$ ground state were observed for Xe−HDO because the partial deuteration reduces the symmetry of the water, and as a result, relaxation from the $\Sigma 1_{01}$ to the $\Sigma 0_{00}$ state is now an allowed process. All measured transition frequencies are listed in Table S6 of the Supporting Information. The nuclear quadrupole hyperfine structures due to the ^{131}Xe and D nuclei were observed and assigned. The determined spectroscopic constants, including the ^{131}Xe and D nuclear quadrupole coupling constants, are given in Table S6 of the Supporting Information.

TABLE 3: Measured Transition Frequencies and Spectroscopic Constants, Including ^{17}O Nuclear Quadrupole Coupling Constants, of Xe−$H_2{}^{17}O$ Isotopomers

			$\Sigma 0_{00}$		$\Sigma 1_{01}$	
	$J'-J''$	$F'-F''$	ν_{obs} (MHz)	$\Delta\nu$ (kHz)[a]	ν_{obs} (MHz)	$\Delta\nu$ (kHz)
^{132}Xe−$H_2{}^{17}O$	2-1	2.5−1.5			7659.7039	−2.2
		3.5−3.5			7659.8755	2.0
		2.5−3.5			7660.0871	4.4
		1.5−1.5			7660.3029	−0.9
		4.5−3.5	7804.4223	0.3	7660.6762	−4.1
		3.5−2.5	7804.4449	−0.6	7660.7506	−1.4
		0.5−1.5	7804.4751	0.2	7660.8423	0.6
		2.5−2.5	7804.5141	0.02	7660.9609	−0.4
		1.5−2.5			7661.5610	2.1
	B/MHz		1951.0981(3)		1915.1473(1)	
	$\chi_{aa}(^{17}O)$/MHz		−1.372(20)		−4.1837(33)	
	δ/kHz[b]		0.4		2.4	
^{129}Xe−$H_2{}^{17}O$	2-1	1.5−1.5			7681.9989	1.7
		4.5−3.5	7827.0133	−0.5	7682.3697	−1.7
		3.5−2.5	7827.0361	−0.7	7682.4397	−3.0
		0.5−1.5	7827.0679	2.4		
		2.5−2.5	7827.1027	−1.2	7682.6536	3.0
	B/MHz		1956.7463(3)		1920.5706(1)	
	$\chi_{aa}(^{17}O)$/MHz		−1.342(20)		−4.157(9)	
	δ/kHz		1.4		2.4	

[a] $\Delta\nu = \nu_{obs} - \nu_{cal}$. [b] Standard deviation of the fit.

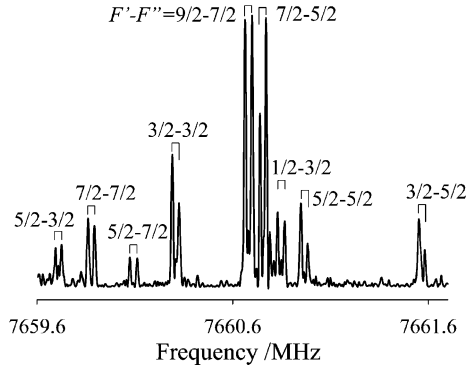

Figure 3. Composite spectrum the $J = 2$-1 transition of the $\Sigma 1_{01}$ state of ^{132}Xe−$H_2{}^{17}O$. A total of 2000 averaging cycles was used to record the spectrum.

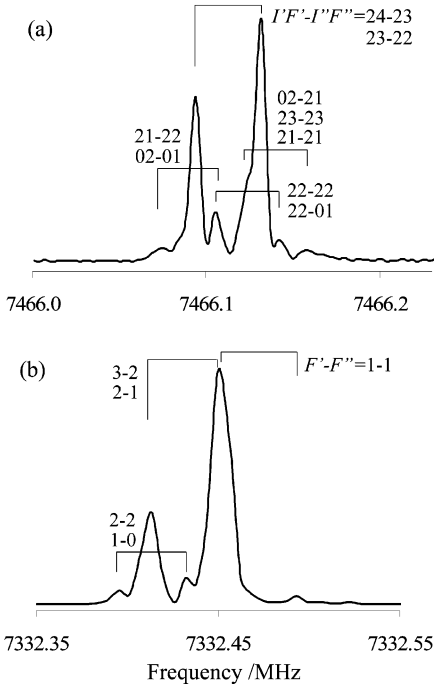

Figure 4. Composite spectra of the $J = 2\text{-}1$ transitions of the $\Sigma 0_{00}$ (a) and $\Sigma 1_{01}$ states (b) of $^{132}Xe-D_2O$. A total of 200 averaging cycles was used in each case.

V. Discussion of ab Initio Results

A 3-dimensional potential energy surface for the $Xe-H_2O$ complex was constructed as function of R, θ, and φ coordinates. A global minimum was found at a planar, hydrogen bonded configuration with $R = 4.0$ Å, $\theta = 60°$, $\varphi = 0°$, and a well depth of -191.7 cm^{-1}. This configuration is rather close to an L-shaped $Xe-HOH$ structure with a linear $Xe-HO$ arrangement. Two first-order saddle points have symmetric $Xe-H_2O$ geometry ($R = 3.95$ Å, $\theta = 0°$, $\varphi = 0°$, -169.1 cm^{-1}) and symmetric $Xe-OH_2$ geometry ($R = 3.85$ Å, $\theta = 180°$, $\varphi = 0°$, -161.5 cm^{-1}), respectively. A second-order saddle point corresponds to a nonplanar configuration with $R = 4.0$ Å, $\theta = 80°$, $\varphi = 90°$ and has an energy of -130.1 cm^{-1}. A minimum energy path was constructed as a function of θ and φ coordinates. At each θ and φ configuration, R was varied to locate the lowest energy. A contour plot of this minimum energy path is shown in Figure 5. This potential has similar overall features as the $Ar-H_2O$ potentials by Cohen et al.,[17] Tao et al.,[20] and Chalasinski et al.[21] Compared with Ar- and $Kr-H_2O$,[17,20,21] the $Xe-H_2O$ equilibrium structure adopts a more hydrogen bonded position (the equilibrium structure of $Ar-H_2O$ was found at $\theta = 74.3°$ in ref 17 and $\theta = 75°$ in ref 20, and $\theta = 80°$ for $Kr-H_2O$ in ref 21), and its potential is slightly more anisotropic in the angular coordinate, implying a more hindered H_2O internal rotation within the $Xe-H_2O$ complex. The potential barrier for the H_2O in-plane rotation is 22.6 cm^{-1} for the symmetric $Xe-H_2O$ geometry ($\theta = 0°$, $\varphi = 0°$) and 30.2 cm^{-1} for the symmetric $Xe-OH_2$ geometry ($\theta = 180°$, $\varphi = 0°$). The barrier to the out-of-plane rotation is 61.6 cm^{-1} ($\theta = 80°$, $\varphi = 90°$).

VI. Discussion of Spectroscopic Results

6.1. Structural Parameters and Force Constants. The rotational constant B and the centrifugal distortion constant D can be used to determine the van der Waals bond length R, the van der Waals stretching frequency ν_s, and the corresponding

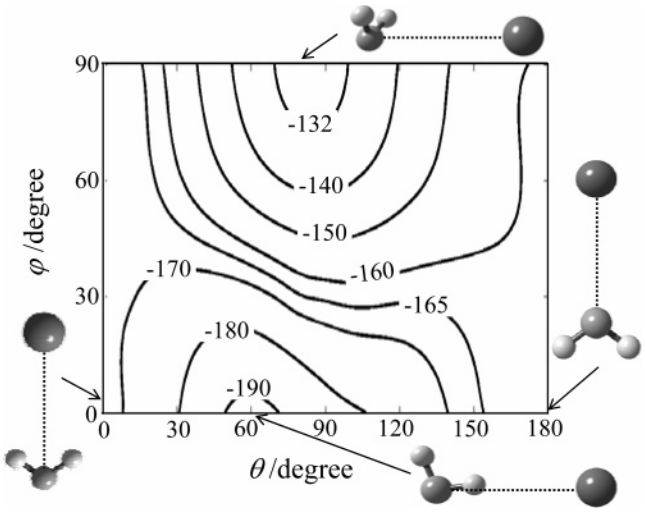

Figure 5. Contour diagram of the ab initio minimum energy path of $Xe-H_2O$ as a function of θ and φ coordinates. R was varied at each θ and φ combination until the lowest energy was found. Energies are given in cm^{-1}.

stretching force constant k_s under the pseudodiatomic approximation,[47]

$$B = h/8\pi^2\mu R^2$$

$$\nu_s = \left(\frac{4B^3}{D}\right)^{1/2}$$

$$k_s = 4\pi^2\nu_s^2\mu \qquad (1)$$

where μ is the pseudodiatomic reduced mass of the complex. The results for the individual isotopomers are listed in Table S7 of the Supporting Information. Values of $R = 3.9485$ Å, $\nu_s = 34.85$ cm^{-1}, and $k_s = 1.134$ N m^{-1} were determined for the $\Sigma 0_{00}$ ground state of $^{132}Xe-H_2O$. This indicates that the van der Waals bond of $^{132}Xe-H_2O$ is slightly longer and more rigid compared to that of $^{84}Kr-H_2O$ ($R = 3.7897$ Å, $\nu_s = 34.8$ cm^{-1}, and $k_s = 1.06$ N m^{-1}).[32] Shorter van der Waals bond lengths and larger force constants were obtained for the deuterated species ($R = 3.9453$ Å, $\nu_s = 34.71$ cm^{-1}, and $k_s = 1.180$ N m^{-1} for the $\Sigma 0_{00}$ state of $^{132}Xe-HDO$; $R = 3.9463$ Å, $\nu_s = 34.84$ cm^{-1}, and $k_s = 1.243$ N m^{-1} for the $\Sigma 0_{00}$ state of $^{132}Xe-D_2O$), in accord with a regular isotope effect. For the $\Sigma 1_{01}$ state, there is an increased van der Waals bond length and a larger force constant compared to the ground state.

An approximate isotopic substitution analysis can be used to derive information about the H_2O orientation with respect to the Xe atom by applying Kraitchman's equations.[48] The assumption that the isotopic substitutions are on the intermolecular a-axis has to be made due to the absence of separated B and C values. This is a good approximation for the ^{18}O substitution because the oxygen atom is rather close to the center-of-mass (c.m.) of the H_2O subunit. Using the rotational constants of the ^{132}Xe containing species, a distance along the a-axis between the center-of-mass of the complex and the oxygen atom was obtained, with values of 3.458 and 3.453 Å, for the $\Sigma 0_{00}$ and $\Sigma 1_{01}$ states, respectively. The hydrogen atoms are further off the a-axis, so that the substitution analysis of their a-coordinates is less accurate. An analysis using data from $^{132}Xe-H_2O$ and $^{132}Xe-D_2O$ gives distances along the a-axis between the center-of-mass of the complex and the hydrogen atoms of 3.452 and 3.455 Å, for the $\Sigma 0_{00}$ and $\Sigma 1_{01}$ states, respectively. The differences between the a-coordinates of the O and H atoms is 0.006 Å for the $\Sigma 0_{00}$ state and 0.002 Å for

TABLE 4: Comparison of ab Initio and Experimental Values of Derived Parameters for $^{132}Xe-H_2O$

		R (Å)	ν_s (cm^{-1})	k_s ($N\ m^{-1}$)
exptl values	$\sum 0_{00}$ state	3.9485	34.85	1.134
	$\sum 1_{01}$ state	3.9875	40.91	1.563
ab initio values	global minimum ($\theta = 60°$, $\varphi = 0°$)	4.0647	43.27	1.748
	first-order saddle point ($\theta = 0°$, $\varphi = 0°$)	4.0251	38.36	1.374
	first-order saddle point ($\theta = 180°$, $\varphi = 0°$)	3.8988	37.28	1.297
	second-order saddle point ($\theta = 80°$, $\varphi = 90°$)	4.0235	32.67	0.997

the $\sum 1_{01}$ state, much smaller compared to the corresponding values in $^{84}Kr-H_2O$ (∼0.05 Å)[32] and Ar−H_2O (∼0.1 Å).[22,23] In the latter cases, it was determined that the H-atoms point on average toward the respective rare gas atom. In the Xe−H_2O case, the difference in the *a*-coordinates of H- and O-atoms is so small that it cannot decide whether the H-atoms point toward or away from the Xe atom. However, it is still worthwhile to point out that these rather small differences in the *a*-coordinates may imply that the anti-hydrogen bonded orientations and nonplanar configurations have more significant contributions to the Xe−H_2O wavefuctions compared to the cases of Kr− and Ar−H_2O.

More information about the motion in the angular coordinates of the Xe−H_2O complex can be obtained from a comparison of spectroscopic and ab initio data. The computer program LEVEL7.5 (ref 49) was used to determine the bound states of $^{132}Xe-H_2O$ that are supported by the ab initio potential curves along radial coordinates at four selected angular configurations (global minimum, two first-order saddle points, and one second-order saddle point), using a pseudodiatomic model. The molecular parameters, R, ν_s, and k_s, were then calculated and are given in Table 4 together with the corresponding experimental values. Those calculated values have the same order of magnitude as the experimental data. The best agreement with the experimental values for the $\sum 0_{00}$ state was found at the symmetric Xe−OH_2 geometry ($\theta = 180°$, $\varphi = 0°$) for R ($\Delta = -1.3\%$) and the second-order saddle point ($\theta = 80°$, $\varphi = 90°$) for ν_s ($\Delta = -6.3\%$) and k_s ($\Delta = -12.1\%$). For the $\sum 1_{01}$ state, the second-order saddle point ($\theta = 80°$, $\varphi = 90°$) gives the R value ($\Delta = +0.9\%$) closest to the experimental values and the global minimum ($\theta = 60°$, $\varphi = 0°$) gives the closet ν_s ($\Delta = +5.8\%$) and k_s ($\Delta = +11.8\%$) values. These variations of discrepancies among different configurations can be considered as a further indication of a rather delocalized Xe−H_2O ground-state wave function. The symmetric Xe−OH_2 geometry ($\theta = 180°$, $\varphi = 0°$) and the second-order saddle point ($\theta = 80°$, $\varphi = 90°$), corresponding to an anti-hydrogen bonded orientation and a nonplanar configuration, respectively, give relatively close values to the experimental ones. This supports what was found in the isotopic substitution analysis, namely that there is a significant contribution to the wave functions in each state from the anti-hydrogen bonded and nonplanar configurations. However, these two methods only gave qualitative information about the H_2O angular motion; more information can be extracted from the hyperfine structure analyses, as discussed in the next session.

6.2. Hyperfine Structure and Angular Information. The observed nuclear quadrupole hyperfine structures due to the presence of the ^{131}Xe, D, and ^{17}O nuclei can be used to deduce dynamical information about the internal angular coordinates of the Xe−H_2O complex. As a result of the large amplitude H_2O internal motions, the orientation of the H_2O unit that we can obtain from the nuclear quadrupole coupling constants χ_{aa} is an effective orientation over these motions. Because H_2O is an asymmetric top, we need to specify two angles (the angle θ between the C_2 axis of H_2O and the intermolecular *a*-axis, and the dihedral angle φ, see Figure 1) to describe its orientation within the complex. To determine both angles, two nuclear quadrupole coupling constants χ_{aa} are needed. Therefore, we utilize the $\chi_{aa}(^{131}Xe)$ value of the $^{131}Xe-H_2O$ isotopomer and $\chi_{aa}(^{17}O)$ of the $^{132}Xe-H_2{}^{17}O$ isotopomer to determine two effective angles θ_{eff} and φ_{eff} in Xe−H_2O, and $\chi_{aa}(^{131}Xe)$ of the $^{131}Xe-D_2O$ isotopomer and $\chi_{aa}(D)$ of the $^{132}Xe-D_2O$ isotopomer to obtain the effective angles in Xe−D_2O. In this procedure, we assume that the isotopic substitutions at the Xe and O position have negligible effect on the dynamics of the complex. In the following section, we will discuss the details of the derivation of the effective angles and interpretation of the results.

6.2.1. Xe−H_2O. The nonzero value of the ^{131}Xe nuclear quadrupole coupling constant $\chi_{aa}(^{131}Xe)$ of $^{131}Xe-H_2O$ arises because the presence of the H_2O molecule distorts spherical symmetry of electron distribution of the Xe atom, which, in turn, results in a nonzero electric field gradient at the Xe nucleus. There are two main contributions to the electric field gradient at the Xe nucleus. One is the dispersion interaction, and the other is the induction interaction between the nonzero electric multipole moments of H_2O and the Xe electron cloud. The labels χ_{dis} and χ_{ind} will be used below to represent the contributions to the quadrupole coupling constant from these two interactions, respectively. In many cases, for example, the $^{131}Xe-HX$ (X = F and Cl) complexes,[9−11] χ_{dis} has been neglected in interpreting the nuclear quadrupole coupling constants because HX (X = F and Cl) has large electric moments so that χ_{dis} is relatively small compared to χ_{ind}. In this picture, the magnitude of the ^{131}Xe nuclear quadrupole coupling constant depends only on the magnitudes of the electric moments of its binding partner and the large amplitude vibrational motions. The electric moments of H_2O are not necessarily smaller than those of HF and HCl. The dipole moment of H_2O (1.855 D) is slightly larger than those of HF (1.826 D) and HCl (1.109 D). However, compared with the $\chi_{aa}(^{131}Xe)$ values of $^{131}Xe-HF$ (−8.54 MHz)[11] and $^{131}Xe-HCl$ (−4.9 MHz),[9,10] the values for $^{131}Xe-H_2O$ (−0.445 MHz for the $\sum 0_{00}$ state and −1.814 MHz for the $\sum 1_{01}$ state) are much smaller. Similar behavior has been found previously in $^{83}Kr-H_2O$. A possible reason is that the electric field gradient at the ^{131}Xe nucleus is reduced by averaging over the large amplitude H_2O internal rotation. The $\chi_{aa}(^{131}Xe)$ value for the $\sum 0_{00}$ state is approximately one-fourth of that of the $\sum 1_{01}$ state, which suggests that H_2O experiences different vibrational dynamics within these two states and might undergo more free internal rotation in the $\sum 0_{00}$ state as indicated by its smaller $\chi_{aa}(^{131}Xe)$ value.

The magnitude of $\chi_{aa}(^{131}Xe)$ for $^{131}Xe-H_2O$ is not much larger than those for $^{131}Xe-{}^{20}Ne$ (0.3878 MHz), $^{131}Xe-Ar$ (0.7228 MHz), and $^{131}Xe-{}^{84}Kr$ (0.7079 MHz), in which cases $\chi_{ind}(^{131}Xe) = 0$.[8] Therefore, we cannot neglect $\chi_{dis}(^{131}Xe)$ in the $^{131}Xe-H_2O$ case. We use the $\chi_{aa}(^{131}Xe)$ value of $^{131}Xe-Ar$, 0.723 MHz as an estimate for $\chi_{dis}(^{131}Xe)$ in $^{131}Xe-H_2O$. In the case of $^{131}Xe-{}^{15}N_2$, $\chi_{dis}(^{131}Xe)$ was estimated to be 0.827 MHz[6] by taking the difference between the experimental $\chi_{aa}(^{131}Xe)$ value and the calculated $\chi_{ind}(^{131}Xe)$ value and was found to be in accord with the $\chi_{aa}(^{131}Xe)$ value of $^{131}Xe-Ar$, 0.723 MHz. The $\chi_{ind}(^{131}Xe)$ values for $^{131}Xe-H_2O$ can be estimated by subtracting $\chi_{dis}(^{131}Xe)$ from the observed $\chi_{aa}(^{131}Xe)$ values, and the resulting values are −1.168 MHz for the $\sum 0_{00}$ state

and −2.537 MHz for the $\sum 1_{01}$ state. These values can be interpreted in terms of the multipole moments of the H_2O monomer using the expressions:[10]

$$q_0 = -6\mu\left\langle\frac{\cos\theta}{R^4}\right\rangle - 12\left\langle\frac{Q_{xx}\sin^2\theta\sin^2\varphi + Q_{yy}\sin^2\theta\cos^2\varphi + Q_{zz}\cos^2\theta}{R^5}\right\rangle - \cdots$$

$$\chi_{ind} = -eq_0(1-\gamma)Q_{Xe}/h \quad (2)$$

In the above expression, q_0 is the electric field gradient generated by the multipole moments of the H_2O monomer at the site of the Xe nucleus. μ and Q are the electric dipole and quadrupole moments of H_2O, respectively, and higher order electric moments have not been considered here. For free H_2O, μ = 1.8546 D[50] and the principal components of the molecular electric quadrupole tensor $Q_{xx} = -2.50$ D Å, $Q_{yy} = 2.63$ D Å, and $Q_{zz} = -0.13$ D Å.[51] The brackets indicate averaging over the large amplitude angular motions. The van der Waals bond length R is 3.9485 Å for the $\sum 0_{00}$ state and 3.9876 Å for the $\sum 1_{01}$ state. The ^{131}Xe nuclear quadrupole moment $Q_{Xe} = -0.12$ b,[52] and the Sternheimer shielding factor $\gamma = -152$.[10]

Because it is impossible to solve for two effective angles θ_{eff} and φ_{eff} only by eq 2, the $\chi_{aa}(^{17}O)$ values of the complex were used to determine an effective orientation of the H_2O unit within the complex. The principal components of the ^{17}O nuclear quadrupole coupling tensor in $H_2{}^{17}O$ are χ_{xx} = 10.169 MHz, $\chi_{yy} = -8.899$ MHz, $\chi_{zz} = -1.269$ MHz.[53] The $\chi_{aa}(^{17}O)$ values for the complex can be expressed as the projection of the monomer constants onto the *a*-axis of the complex, under the assumption that the monomer constants remain unchanged upon complex formation.

$$\chi_{aa}(^{17}O) = \chi_{xx}\langle\sin^2\theta\sin^2\varphi\rangle + \chi_{yy}\langle\sin^2\theta\cos^2\varphi\rangle + \chi_{zz}\langle\cos^2\theta\rangle \quad (3)$$

For ^{132}Xe−$H_2{}^{17}O$, the $\chi_{aa}(^{17}O)$ values are −1.372 and −4.184 MHz for the $\sum 0_{00}$ and $\sum 1_{01}$ states, respectively. These quite different $\chi_{aa}(^{17}O)$ values are further evidence for different vibrational dynamics in the two states. Similar observations were reported previously, for CO−H_2O,[54] Ar−H_2O,[22,23] Kr−H_2O,[32] and Ne−H_2S.[55] In the limit of free rotation of the H_2O monomer, the $\chi_{aa}(^{17}O)$ value is zero. A smaller $\chi_{aa}(^{17}O)$ value in the $\sum 0_{00}$ state than the $\sum 1_{01}$ state suggests more free H_2O internal rotation in the $\sum 0_{00}$ state, also consistent with the observed smaller $\chi_{aa}(^{131}Xe)$ value in the $\sum 0_{00}$ state. Equations 2 and 3 can be solved for the effective angles θ_{eff} and φ_{eff} by neglecting the averaging brackets. The obtained values are $\theta_{eff} = 88.5°$, $\varphi_{eff} = 38.9°$ for the $\sum 0_{00}$ state and $\theta_{eff} = 86.2°$, $\varphi_{eff} = 29.8°$ for the $\sum 1_{01}$ state. These orientations are between hydrogen bonded and anti-hydrogen bonded orientations. This might suggest that the hydrogen bonded and anti-hydrogen bonded orientations have similar contributions to the Xe−H_2O wave function in each state. This is further supported by the similar energy barriers to the symmetric Xe−H_2O geometry (hydrogen bonded orientation, 22.6 cm^{-1}) and Xe−OH_2 geometry (anti-hydrogen bonded orientation, 30.2 cm^{-1}) in the ab initio potential. The large amplitude out-of-plane motion is evident from the obtained φ_{eff} values, and this is consistent with the structural parameters and force constants obtained from the rotational and distortion constants.

6.2.2. Xe−D_2O and Xe−HDO. Assuming that the nuclear quadrupole coupling constants for free D_2O and HDO are not affected by complex formation, the determined $\chi_{aa}(D)$ constants for the complex can also be interpreted in terms of projection of monomer constants. Different from the ^{17}O case, the D nuclear quadrupole coupling tensors in D_2O and HDO are quite symmetric (η = 0.06 for D_2O, η = 0.11 for HDO), and the following expressions can be used under the assumption that the quadrupole interaction is cylindrically symmetric about the O−D bond:

$$\chi_{aa}(D) = \frac{1}{2}\chi_0\langle 3\cos^2\beta - 1\rangle \quad (4)$$

Here, β is the angle between the O−D bond axis and the *a*-axis of the complex. χ_0 is the principal component of the D nuclear quadrupole coupling tensor along the O−D bond, $\chi_0(D_2O)$ = 0.330 MHz[54] and χ_0(HDO) = 0.313 MHz.[54,56] The brackets indicate averaging over the large amplitude angular motions. From eq 4, we calculated $\langle\cos^2\beta\rangle$ values to be 0.437 for the $\sum 0_{00}$ state [$\chi_{aa}(D)$ = 0.0513(12) MHz] and 0.479 for the $\sum 1_{01}$ state [$\chi_{aa}(D)$ = 0.0726(14) MHz] of ^{132}Xe−D_2O and 0.432 for ^{132}Xe−HDO [$\chi_{aa}(D)$ = 0.0464(16) MHz]. These values are relatively close to the $\langle\cos^2\beta\rangle$ value of 0.333 in the free rotor limit, which may indicate that the D_2O and HDO units undergo only slightly hindered internal rotation within the complexes. The obtained effective angles β_{eff} are 48.6°, 131.4° for the $\sum 0_{00}$ state and 46.2°, 133.8° for the $\sum 1_{01}$ state of ^{132}Xe−D_2O and 48.9°, 131.1° for ^{132}Xe−HDO. At first glance, the two internal rotor states of ^{132}Xe−D_2O have similar dynamics because the difference in β_{eff} is only 2.4°. This is similar to the CO−H_2O,[54] Ar−H_2O,[22,23] Kr−H_2O,[32] and Ne−H_2S[55] cases. However, it appears to contradict our findings from the ^{131}Xe hyperfine structures in the ^{131}Xe−D_2O. The $\chi_{aa}(^{131}Xe)$ values are −1.449 MHz for the $\sum 0_{00}$ state and −2.76 MHz for the $\sum 1_{01}$ state and imply different dynamics for the two states, consistent with the observations in the ^{131}Xe−H_2O complex. A possible reason for this contradiction is that the $\chi_{aa}(D)$ values are primarily sensitive to the projection of the O−D bond onto the *a*-axis of the complex, and insensitive to the D_2O out-of-plane motion, as suggested by Yaron et al.[54]

To better understand the dynamics of Xe−D_2O, we can determine effective angles θ_{eff} and φ_{eff} from both the $\chi_{aa}(D)$ and $\chi_{aa}(^{131}Xe)$ constants. The $\chi_{ind}(^{131}Xe)$ values of ^{131}Xe−D_2O were obtained by following the same procedure as for ^{131}Xe−H_2O and the estimated $\chi_{dis}(^{131}Xe)$ value, 0.723 MHz, was used. Equation 2 is still applicable here to relate the $\chi_{ind}(^{131}Xe)$ values to the respective angles, with μ = 1.8545 D,[50] $Q_{xx} = -2.402$ D Å, Q_{yy} = 2.724 D Å, and $Q_{zz} = -0.321$ D Å,[51] and R = 3.9463 Å ($\sum 0_{00}$ state) and 3.9823 Å ($\sum 1_{01}$ state). Because angles θ and φ are not included in eq 4, they cannot be obtained directly by solving eqs 2 and 4. Instead, the θ_{eff} and φ_{eff} were determined by looking for the orientations that satisfied eq 2 and can also reproduce the angle β_{eff} obtained from eq 4. This yields values of $\theta_{eff} = 89.9°$, $\varphi_{eff} = 31.9°$ for the $\sum 0_{00}$ state and $\theta_{eff} = 87.2°$, $\varphi_{eff} = 21.9°$ for the $\sum 1_{01}$ state. Note that there is more than one pair of θ_{eff} and φ_{eff} values obtained for each state, but only the values closest to those for Xe−H_2O are reported here under the assumption that the vibrational dynamics does not change dramatically upon deuteration. The resulting φ_{eff} value has a 10.0° difference for the two states, similar to the Xe−H_2O case. This result also supports that the $\chi_{aa}(D)$ value is not sensitive to the out-of-plane motion of H_2O.

VII. Summary and Conclusions

A 3-dimensional ab initio potential energy surface of Xe−H_2O complex was constructed at the CCSD(T) level of theory.

The global minimum corresponds to a planar, hydrogen bonded configuration, close to the L-shaped Xe−HOH structure with a linear Xe−HO arrangement. The potential barrier was found to be lower for the H_2O in-plane rotation compared to the out-of-plane motion. Rotational spectra of the Xe−H_2O complex were recorded using a Fourier transform microwave spectrometer. Transitions within two internal rotor states, namely, the $\Sigma 0_{00}$ and $\Sigma 1_{01}$ states, were measured and assigned. Nuclear quadrupole hyperfine structures due to the presence of the ^{131}Xe ($I = {}^3/_2$), D ($I = 1$) and ^{17}O ($I = {}^5/_2$) nuclei were observed and analyzed. The obtained structural parameters and force constants suggest that the ground-state wave function for Xe−H_2O is rather delocalized in the angular coordinates and that the anti-hydrogen bonded orientations and nonplanar configurations have significant contribution to the wave function. The hyperfine structure analysis was used to derive the information about the vibrational dynamics of the Xe−H_2O and Xe−D_2O complex. The nuclear quadrupole coupling constants for ^{131}Xe and ^{17}O indicate that the two internal rotor states have different dynamics and that the $\Sigma 0_{00}$ state undergoes less hindered internal motion of the water unit. The obtained effective H_2O orientations also support the significant contribution to the wave functions in each state from the anti-hydrogen bonded orientations and nonplanar configurations and are in agreement with the structural parameters and force constants obtained from the rotational and centrifugal distortion constants.

Acknowledgment. This work was funded by the Natural Sciences and Engineering Research Council of Canada. We thank Wendy Topic for helpful discussions and suggestions.

Supporting Information Available: Tables with additional transition frequencies, quantum number assignments, spectroscopic constants, structural parameters, force constants, and ab initio data points for the potential energy surfaces. Figure of the composite spectrum of the $J = 1$-0 transition of the $\Sigma 1_{01}$ state of ^{132}Xe−H_2O. This material is available free of charge via the Internet at http://pubs.acs.org.

References and Notes

(1) Navon, G.; Song, Y.-Q.; Room, T.; Appelt, S.; Taylor, R. E.; Pines, A. *Science* **1996**, *271*, 1848.
(2) Goodson, B. M. *J. Magn. Reson.* **2002**, *155*, 157.
(3) Song, Y.-Q. *Concept. Magn. Res.* **2000**, *12*, 6.
(4) Bonardet, J.-L.; Fraissard, J.; Gédéon, A.; Springuel-Huet, M.-A. *Catal. Rev.-Sci. Eng.* **1999**, *41*, 115.
(5) Sears, D. N.; Jameson, C. J. *J. Chem. Phys.* **2004**, *121*, 2151.
(6) Wen, Q.; Jäger, W. *J. Chem. Phys.* **2005**, *122*, 214310.
(7) Wen, Q.; Jäger, W. *J. Chem. Phys.* **2006**, *124*, 014301.
(8) Jäger, W.; Xu, Y.; Gerry, M. C. L. *J. Chem. Phys.* **1993**, *99*, 919.
(9) Keenan, M. R.; Buxton, L. W.; Campbell, E. J.; Balle, T. J.; Flygare, W. H. *J. Chem. Phys.* **1980**, *73*, 3523.
(10) Campbell, E. J.; Buxton, L. W.; Keenan, M. R.; Flygare, W. H. *Phys. Rev. A* **1981**, *24*, 812.
(11) Baiocchi, F. A.; Dixon, T. A.; Joyner, C. H.; Klemperer, W. *J. Chem. Phys.* **1981**, *75*, 2041.
(12) Iida, M.; Ohshima, Y.; Endo, Y. *J. Phys. Chem.* **1993**, *97*, 357.
(13) Walker, K. A.; Ogata, T.; Jäger, W.; Gerry, M. C. L.; Ozier, I. *J. Chem. Phys.* **1997**, *106*, 7519.
(14) Brupbacher, Th.; Makarewicz, J.; Bauder, A. *J. Chem. Phys.* **1994**, *101*, 9736.
(15) Hutson, J. *J. Chem. Phys.* **1990**, *92*, 157.
(16) Cohen, R. C.; Saykally, R. J. *J. Phys. Chem.* **1990**, *94*, 7991.
(17) Cohen, R. C.; Saykally, R. J. *J. Chem. Phys.* **1993**, *98*, 6007.
(18) Chalasinski, G.; Szczesniak, M. M.; Scheiner, S. *J. Chem. Phys.* **1991**, *94*, 2807.
(19) Bulski, M.; Wormer, P. E. S.; van der Avoird, A. *J. Chem. Phys.* **1991**, *94*, 8096.
(20) Tao, F.-M.; Klemperer, W. *J. Chem. Phys.* **1994**, *101*, 1129.
(21) Chalasinski, G.; Szczesniak, M. M.; Scheiner, S. *J. Chem. Phys.* **1992**, *97*, 8181.
(22) Fraser, G. T.; Lovas, F. J.; Suenram, R. D.; Matsumura, K. *J. Mol. Spectrosc.* **1990**, *144*, 97.
(23) Germann, T. C.; Gutowsky, H. S. *J. Chem. Phys.* **1993**, *98*, 5235.
(24) Cohen, R. C.; Busarow, K. L.; Laughlin, K. B.; Blake, G. A.; Havenith, M.; Lee, Y. T.; Saykally, R. J. *J. Chem. Phys.* **1988**, *89*, 4494.
(25) Cohen, R. C.; Busarow, K. L.; Lee, Y. T.; Saykally, R. J. *J. Chem. Phys.* **1990**, *92*, 169.
(26) Cohen, R. C.; Saykally, R. J. *J. Chem. Phys.* **1991**, *95*, 7891.
(27) Suzuki, S.; Bumgarner, R. E.; Stockman, P. A.; Green, P. G.; Blake, G. A. *J. Chem. Phys.* **1991**, *94*, 824.
(28) Zwart, E.; Meerts, W. L. *Chem. Phys.* **1991**, *151*, 407.
(29) Weida, M. J.; Nesbitt, D. J. *J. Chem. Phys.* **1997**, *106*, 3078.
(30) Lascola, R.; Nesbitt, D. J. *J. Chem. Phys.* **1991**, *95*, 7917.
(31) Nesbitt, D. J.; Lascola, R. *J. Chem. Phys.* **1992**, *97*, 8096.
(32) van Wijngaarden, J.; Jäger, W. *Mol. Phys.* **2000**, *98*, 1575.
(33) MOLPRO, a package of ab initio programs designed by Werner, H.-J. and Knowles, P. J. version 2002.6, with contributions by J. Almlof, R. D. Amos, A. Berning, et al.
(34) Knowles, P. J.; Hampel, C.; Werner, H.-J. *J. Chem. Phys.* **1993**, *99*, 5219.
(35) Deegan, M. J. O.; Knowles, P. J. *Chem. Phys. Lett.* **1994**, *227*, 321.
(36) Peterson, K. A.; Figgen, D.; Goll, E.; Stoll, H.; Dolg, M. *J. Chem. Phys.* **2003**, *119*, 11113.
(37) Dunning, T. H., Jr. *J. Chem. Phys.* **1989**, *90*, 1007.
(38) Tao, F.-M.; Pan, Y.-K. *Chem. Phys. Lett.* **1992**, *194*, 162.
(39) Cybulski, S. M.; Toczylowski, R. R. *J. Chem. Phys.* **1999**, *111*, 10520.
(40) Boys, S. F.; Bernadi, F. *Mol. Phys.* **1970**, *19*, 553.
(41) Liu, B.; Mclean, A. D. *J. Chem. Phys.* **1973**, *59*, 4557.
(42) Lide, D. R. *CRC Handbook of Chemistry and Physics*, 84th ed.; CRC: Boca Raton, FL, 2003.
(43) Balle, T. J.; Flygare, W. H. *Rev. Sci. Instrum.* **1981**, *52*, 33.
(44) Xu, Y.; Jäger, W. *J. Chem. Phys.* **1997**, *106*, 7968.
(45) Gutowsky, H. S.; Emilsson, T.; Arunan, E. *J. Chem. Phys.* **1997**, *106*, 5309.
(46) Pickett, H. M. *J. Mol. Spectrosc.* **1991**, *148*, 371.
(47) Gordy, W.; Cook, R. L. *Microwave Molecular Spectra*, 3rd ed.; Wiley: London, 1984.
(48) Kraitchman, J. *Am. J. Phys.* **1953**, *21*, 17.
(49) LeRoy, R. J. "LEVEL7.5, *A Computer Program for Solving the Radial Schrödinger Equation for Bound and Quasibound Levels*," University of Waterloo, Chemical Physics Research Report No. CP-655, 2002.
(50) Dyke, T. R.; Muenter, J. S. *J. Chem. Phys.* **1973**, *59*, 3125.
(51) Verhoeven, J.; Dymanus, A. *J. Chem. Phys.* **1970**, *52*, 3222.
(52) Faust, W. L.; McDermott, M. N. *Phys. Rev.* **1961**, *123*, 198.
(53) De Lucia, F. C.; Helminger, P. *J. Mol. Spectrosc.* **1975**, *56*, 138.
(54) Yaron, D.; Peterson, K. I.; Zolandz, D.; Klemperer, W.; Lovas, F. J.; Suenram, R. D. *J. Chem. Phys.* **1990**, *92*, 7095.
(55) Liu, Y.; Jäger, W. *Mol. Phys.* **2002**, *100*, 611.
(56) Fry, H. A.; Kukolich, S. G. *J. Chem. Phys.* **1982**, *76*, 4387.